

**Beam-beam mode coupling in collision with a crossing angle**Kazuhiro Ohmi,<sup>1,2</sup> Yuan Zhang,<sup>1</sup> and Chuntao Lin<sup>3</sup><sup>1</sup>*IHEP, Institute of High Energy Physics, Yuquan Road Beijing 100049, China*<sup>2</sup>*KEK, High Energy Accelerator Organization, Tsukuba, Ibaraki 305-0801, Japan*<sup>3</sup>*Institute of Advanced Science Facilities, Shenzhen, Guangdong, 518107, China*

(Received 3 June 2023; accepted 19 October 2023; published 2 November 2023)

In recent  $e^+e^-$  colliders, a collision scheme with a large crossing angle has been designed and adopted. In two colliding beams, mode coupling between beam-beam oscillation modes is discussed in this paper. The typical  $\sigma$  and  $\pi$  modes are extended to include longitudinal motion. The tune shifts of the  $l = 0$  and  $l = \pm 1$  modes are presented explicitly. The behavior of beam-beam modes is analyzed for different Piwinski angles. The instability due to the vacuum pipe impedance is discussed in terms of mode coupling between these beam-beam modes. Beam-beam simulations based on the strong-strong model have shown that a vertical beam-beam instability is induced by crosstalk between the beam-beam collision and the impedance. It is shown that the mode coupling theory for colliding beams reproduces the results of the beam-beam simulation. The impact of hourglass effects on the instability is also studied by simulation.

DOI: [10.1103/PhysRevAccelBeams.26.111001](https://doi.org/10.1103/PhysRevAccelBeams.26.111001)**I. INTRODUCTION**

There are various modes for inner bunch oscillation. We focus on the vertical motion correlated to longitudinal motion. The target of this study is solving for the transverse dipole amplitude  $y$  in the longitudinal phase space  $[y(z, \delta)]$  in collider accelerators. The bunch oscillates with betatron tune  $\nu_\beta$  in the vertical while rotating with the synchrotron tune in the longitudinal phase space  $z - \delta$ . The vertical amplitude has periodicities in azimuthal on the longitudinal phase space. The amplitude is expressed by the Fourier component on the azimuthal angle,  $y(z, \delta) = y_l e^{il\phi}$ . A bunch with this structure oscillates in the vertical with tune  $\nu_\beta + l\nu_s$ .

Transverse mode coupling instability (TMCI) is caused by the merging of two of these oscillation modes [1]. A typical case is that tunes of modes with  $l = 0$  and  $l = -1$  shift from  $\nu_\beta + l\nu_s$  due to interaction with the beam pipe environment: that is impedance. The two tunes merge into a value at a certain beam intensity, and then the appearance of an imaginary part of the tune results in an instability.

Considering colliding beams, the oscillation modes of the two beams are coupled.  $\sigma$  and  $\pi$  modes with  $y^{(+)} = y^{(-)}$  and  $y^{(+)} = -y^{(-)}$  are well known. Considering longitudinal direction,  $\sigma$  and  $\pi$  modes with  $y^{(+)}(z) = y^{(-)}(z)$  and

$y^{(+)}(z) = -y^{(-)}(z)$  are discussed recently. Horizontal beam-beam instability has been studied for the modes [2–4]. The horizontal instability has been discussed only for the beam-beam interaction with a large crossing angle. The vertical beam-beam instability has begun to be explored with coupling to the vacuum pipe impedance recently [5–8]. In the horizontal, coupling of a mode with the wrapped mode at the half-integer [2,3] causes the instability.  $e^+e^-$  colliders operated at a horizontal tune closed to a half-integer. The wrapped mode occurs because the beam-beam force is localized and the tune is folded at half-integer. On the other hand, the vertical tune is far away from a half-integer. The azimuthal mode numbers, that cause coupling, are higher than horizontal. We discuss here the coupling between lower azimuthal modes as a combined effect of the beam-beam and impedance.

Historically, the beam-beam mode in head-on collision has been discussed in Ref. [9] and mode coupling of the beam-beam modes has been discussed in Ref. [10]. The new aspect of this paper is the extension of this theory into recent/future colliders operated with a large crossing angle.

We first discuss beam-beam modes only under the beam-beam interaction. The cross-wake force is used to analyze the beam-beam modes. Instability does not appear in low azimuthal modes, because the cross-wake impedance is pure imaginary. Then beam-beam modes including impedance from the vacuum environment are discussed taking care of how instability occurs in the beam-beam modes. Strong-strong simulation results, which focus on the instability theory, are presented combined with a beam-beam collision with a large crossing angle and transverse conventional wake force.

*Published by the American Physical Society under the terms of the Creative Commons Attribution 4.0 International license. Further distribution of this work must maintain attribution to the author(s) and the published article's title, journal citation, and DOI.*

## II. TRANSVERSE MODE ANALYSIS FOR COLLIDING BEAMS

We discuss beam-beam mode for colliding  $e^\pm$  beams using the cross-wake force. The transparency condition is assumed for simplicity: i.e., energy transparency  $N^{(+)}\gamma^{(+)} = N^{(-)}\gamma^{(-)}$ , equal beam sizes  $\sigma_{x,y,z}^{(+)} = \sigma_{x,y,z}^{(-)}$ , and equal tunes  $\nu_{x,y,z}^{(+)} = \nu_{x,y,z}^{(-)}$ .

During the collision, the equation of motion for the dipole amplitude distribution  $y(z), p_y(z)$  is expressed by

$$\delta p_y^{(+)}(z) = \int W_{y,\text{crs}}^{(+)}(z-z')\rho^{(-)}(z')dz' \times [y^{(+)}(z) - y^{(-)}(z')], \quad (1)$$

where  $W_{y,\text{crs}}$ , which is called the cross-wake force, represents a longitudinal correlation in the overlap area of the two beams with a half-crossing angle  $\theta$  [2,3,7],

$$W_{y,\text{crs}}^{(+)}(z) = -\frac{N^{(-)}r_e}{\gamma^{(+)}} \frac{\partial F_y(\theta z)}{\partial y} \approx -\frac{N^{(-)}r_e}{\gamma^{(+)}} \frac{1}{\sigma_x\sigma_y(s)} \exp\left(-\frac{\theta_P^2 z^2}{4\sigma_z^2}\right), \quad (2)$$

where  $\theta_P = \theta\sigma_z/\sigma_x$  is known as the Piwinski angle [11]. It is a normalized crossing angle, which is the ratio of the bunch length and overlap area in collision. The corresponding impedance is expressed by

$$Z_{\text{crs}}(\omega) = i \int W_{y,\text{crs}}(z) e^{-i\omega z/c} dz/c = -i \frac{N^{(-)}r_e}{\gamma^{(+)}} \frac{1}{\sigma_x\sigma_y(s)} \frac{\sqrt{4\pi}\sigma_z}{c\theta_P} \exp\left(-\frac{\omega^2\sigma_z^2}{c^2\theta_P^2}\right). \quad (3)$$

Here the hourglass effect due to the vertical beta variation and beam disruption during the collision is neglected.

We introduce beam-beam modes of  $\sigma$  and  $\pi$  modes, which satisfy  $y^{(+)}(z) = y^{(-)}(z)$  and  $y^{(+)}(z) = -y^{(-)}(z)$ . Equation (1) is expressed as single beam equation,

$$\delta p_y(z) = \int W_{y,\text{crs}}(z-z')\rho(z')dz'[y(z) \mp y(z')], \quad (4)$$

where  $\mp$  corresponds to  $\sigma/\pi$  mode.

This equation is the same as that for traditional wakefield containing quadrupole component ( $W_Q$ ) induced by monopole moment  $\rho(z)$  and dipole component ( $W_D$ ) induced by dipole moment  $\rho_y(z) = y(z)\rho(z)$ .

Considering the wake force induced by the vacuum pipe environment,  $W_y$  and  $W_{y,Q}$ , the wake forces of quadrupole and dipole components are  $W_Q = -W_{y,\text{crs}} + W_{y,Q}$ ,  $W_D = \pm W_{y,\text{crs}} + W_y$ .

The dipole amplitudes are extended as functions of longitudinal canonical variables,  $(z, \delta)$  or  $(J, \phi)$ .  $y(z) = \int y(z, \delta)\psi(z, \delta)d\delta / \int \psi(z, \delta)d\delta$ , where  $\psi(z, \delta)$  is the distribution function in the longitudinal phase space. Equation (1) is extended by keeping the same form because it does not contain  $\delta$ . The dipole amplitudes, which are normalized by  $\beta_y^*$  (beta function at the interaction point), are expanded into azimuthal modes

$$\frac{y^*(z, \delta)}{\sqrt{\beta_y^*}} = \sum_{l=-\infty}^{\infty} y_l(J) e^{il\phi}, \quad \sqrt{\beta_y^*} p_y^*(z, \delta) = \sum_l p_l(J) e^{il\phi}. \quad (5)$$

For the longitudinal motion with an elliptic trajectory, the relation between  $(z, \delta)$  and  $(J, \phi)$  is  $z = \sqrt{2\beta_z J} \cos \phi$  and  $\delta = \sqrt{2J/\beta_z} \sin \phi$ . The equation for azimuthal modes is expressed as

$$\delta p_l(J) = -\beta_y^* \left[ \sum_{l'} \bar{W}_{ll'}(J) y_{l'}(J) + \int \sum_{l'} W_{ll'}(J, J') \psi(J') y_{l'}(J') dJ' \right], \quad (6)$$

where

$$\bar{W}_{ll'}(J) = \frac{1}{2\pi} \int \psi(J') dJ' d\phi d\phi' W_Q(z-z') e^{-i(l-l')\phi}, \quad (7)$$

$$W_{ll'}(J, J') = \frac{1}{2\pi} \int d\phi d\phi' W_D(z-z') e^{-il\phi + il'\phi'}. \quad (8)$$

The integration regions are 0 to  $2\pi$  for  $\phi, \phi'$ , and 0 to  $\infty$  for  $J'$ . Equation (6) is regarded as a matrix equation discretized in  $J$ . The revolution matrix containing the wake forces is constructed by combining the transfer matrix of the arc as a function of  $\nu_y$  and  $\nu_s$ . The matrix size is  $2 \times (2l_{\text{max}} + 1) \times n_J$ , where the summation is truncated to  $l = \pm l_{\text{max}}$  and an integral is performed with  $n_J$  steps.

Here we consider a simple radial mode as in [1]

$$y_l(J) = y_{l0} \hat{J}^{|l|/2} / \sqrt{|l|!}, \quad (9)$$

where  $\hat{J} = J/\varepsilon$  is normalized by the longitudinal emittance. The modes are drawn as a flat disk with an undulation with waves of  $l$  periods azimuthally in  $z - \delta - y$  space. The matrix relation for the azimuthal modes is expressed by

$$\delta p_{l0} = \sum_{l'} M_{w, ll'} y_{l'0}. \quad (10)$$

The matrix is expressed by

$$\begin{aligned}
 M_{W,l'l'} &= \frac{i\beta_y^*}{2\pi\sqrt{|l'!|l'!}} \int d\omega \\
 &\times \left[ i^{l-l'} Z_Q(\omega) \int dJ e^{-J} J^{(|l+l'|)/2} J_{l-l'}(k_\sigma r) e^{-k_\sigma^2/2} \right. \\
 &\left. + i^{|l-l'|} Z_D(\omega) (k_\sigma/\sqrt{2})^{|l+l'|} e^{-k_\sigma^2} \right], \quad (11)
 \end{aligned}$$

where  $r = \sqrt{2J}$ . The size of the matrix is  $2 \times (2l_{\max} + 1)$ .

The diagonal term of the matrix gives the tune shift for each azimuthal mode. We first take a look at the tune shift caused by the cross-wake force in Eqs. (2) and (3). The tune shift for  $l = \pm n$  mode is given by

$$\begin{aligned}
 \Delta\nu_{y,\pm n} &= \frac{\beta_y^*}{4\pi} \frac{i}{2\pi n!} \int d\omega Z_{\text{crs}}(\omega) \\
 &\times [n! L_n(k_\sigma^2/2) \mp (k_\sigma/\sqrt{2})^{2n}] e^{-k_\sigma^2}, \quad (12)
 \end{aligned}$$

where  $k_\sigma = \omega\sigma_z/c$ .  $L_n$  is the  $n$ th order Laguerre polynomial. The tune shifts of  $l = 0$  and  $\pm 1$  modes are expressed by

$$\Delta\nu_{y,0} = \frac{\xi}{2} \begin{cases} 0 \\ 2 \end{cases} \quad \Delta\nu_{y,1} = \frac{\xi}{2} \begin{cases} \frac{\theta_p^2/2+1}{1+\theta_p^2} \\ 1 \end{cases}, \quad (13)$$

where upper/lower are values of  $\sigma/\pi$  mode, respectively.  $\xi$  is so-called the beam-beam parameter (tune shift),

$$\xi = \frac{\beta_y^* N r_e}{2\pi} \frac{1}{\gamma \sigma_x \sigma_y \sqrt{1 + \theta_p^2}}. \quad (14)$$

Considering the wake force from the vacuum environment, the tune shift is the summation of this tune shift with  $W_{y,\text{crs}}$  and the ordinary current dependent tune shift.

### A. Beam-beam modes of colliding beams

Beam-beam modes of colliding beams are obtained by solving the eigenvalue problem for the revolution matrix constructed from Eq. (6) and the arc transfer matrix, which is described by  $\nu_\beta$  and  $\nu_s$ . The radial mode is expanded using, for example, Laguerre polynomials in traditional works [1]. It does not seem that the polynomials are suitable in our case, thus the radial mode is directly represented by discretized  $J$ . Here the integration with respect to  $J$  is performed in the region of  $\sqrt{2J_{\max}/\varepsilon_z} = \sqrt{6} = 2.45$  in  $n_J = 40$  or 80 steps.

Parameters used are based on those of SuperKEKB at 2022:  $\xi = 0.07$  at the bunch populations  $N_{+/-} = 9.3/5.3 \times 10^{10}$  for the positron/electron beam, where the energies are  $E_{+/-} = 4/7$  GeV. The vertical and synchrotron tunes are  $\nu_y = 0.592$  and  $\nu_s = 0.023$ . The Piwinski angle is  $\theta_p = 12$ , where the bunch length  $\sigma_z = 6$  mm.  $\beta_y$  is

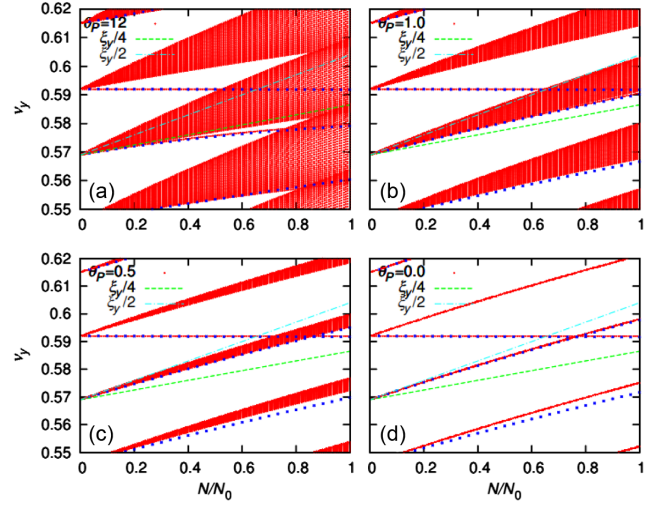


FIG. 1. Tune variation of beam-beam  $\sigma$  modes for the beam-beam cross wake as functions of bunch population. Plots (a)–(d) show tune variation for  $\theta_p = 12, 1, 0.5, 0$ , respectively. The blue dots are given for the flat mode in Eqs. (9) and (11). Lines for  $\xi/2$  (green) and  $\xi/4$  (cyan) are drawn.

1 mm, so the ratio of  $\beta_y$  and the overlap area during collision is  $\beta_y\theta/\sigma_x = \beta_y\theta_p/\sigma_z = 2.3$ . Actually, the parameters used in the analysis are  $\xi$ ,  $\theta_p$ , and the tunes.

Figure 1 presents tune variation of beam-beam  $\sigma$  modes as functions of bunch population, where  $\xi = 0.07$  for  $N/N_0 = 1$ . Eigenvalues are calculated for five values of  $\theta_p$ . Plots (a)–(d) show tune, which is the real part of the eigenvalues divided by  $2\pi$ , for  $\theta_p = 12, 1.0, 0.5, 0.0$ , respectively. The tune behavior for  $\theta_p = 3$ , which is not presented here, is almost the same as that of  $\theta_p = 12$ .  $\beta_y$  and  $\varepsilon_y$  are chosen so that  $\xi$  and  $\sigma_z$  are kept while changing  $\theta_p$ . The imaginary part of the eigenvalues, which are the growth rate of the eigenmodes, is zero: that is stable for the cross wake. The imaginary part (growth) can appear as mode coupling with wrapped modes at half or integer tune [2] as is discussed in Sec. I. We here treat the azimuthal modes  $l_{\max} = 4$  to avoid the wrapped mode. The azimuthal mode number is 5 or more for  $\nu_y = 0.592$ ,  $\nu_s = 0.023$ , which leads to the coupling of a mode with the wrapped mode at the half-integer can cause the instability theoretically. Actually, instabilities have not been seen for beam-beam simulations without vacuum environment wake in the present parameter space. Perhaps the wrapped modes are smeared because of the high azimuthal mode number. Detailed discussions are seen in Ref. [7].

For zero crossing angle, the cross-wake force is constant in  $z$ . All radial modes with the same azimuthal mode number are degenerated as shown in plot (d). The tune is constant for  $\xi$  in  $l = 0$  mode, while  $\Delta\nu = \xi/2$  in  $l \neq 0$  modes.

There are  $n_J$  points for each azimuthal mode in each  $N/N_0$ . The eigenvectors showed that each point corresponded to a certain  $J$ . Namely, the tunes continuously

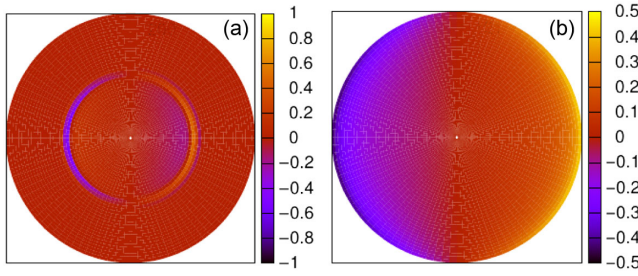


FIG. 2. Dipole amplitude distributions in the longitudinal phase space ( $\pm 2.45\sigma$ ) calculated by eigenvectors. Plots (a) and (b) are drawn for an intermediate tune and for the isolated mode, respectively.

distributed as a function of  $J$ . The tune of all azimuthal modes spreads for increasing  $\xi$  as shown in plots (a)–(c). The eigenvectors also showed that tune and/or tune shift is larger for smaller  $J$ . The spread is narrower for decreasing  $\theta_p$  and disappear at  $\theta_p = 0$  discussed above.

There is an isolated mode at  $\nu_y$  independent of  $\xi$  in plots (a)–(c). Another isolated mode with the tune  $\nu_y - \nu_s$  is seen in plots (a) and (b). The mode tune increases proportionally to  $\xi/4$  at small bunch population  $N/N_0 \leq 0.2$ . The behavior is consistent with Eq. (13). After that, the tune increases slowly compared to  $\xi/4$  and splits from other modes for increasing  $N/N_0$ .

The mode analysis is also performed using the flat radial mode in Eq. (9). The matrix in Eq. (11) is used for solving eigenmodes. The eigenvalues are plotted in Fig. 1 as blue points. For  $l = 0$  and  $-1$  modes, the tunes completely agree with those of the isolated modes. It is shown that the isolated modes at  $l = 0$  and  $l = -1$  correspond to the flat modes  $y_{00}$  and  $y_{-10}$  in Eq. (9). There are some discrepancies in  $l = -2$  or lesser modes. It is likely that those modes are deviated from a flat distribution in Eq. (9).

Figure 2 presents examples of eigenvectors of the modes with  $l = -1$ . The vertical amplitude  $y(z, \delta)$  in the longitudinal phase space ( $\pm 2.45\sigma$ ) is reconstructed by the eigenvector. Plot (a) was obtained from an eigenvector in  $J$  around the middle of the distributed tune in Fig. 1(a). The distribution contains a thin skin component along the circumference in the corresponding  $J$ . The left and right sides are deviated in negative and positive  $y$ . Plot (b) was obtained from the eigenvector of the isolated mode. The dipole amplitude distributes smoothly from negative to positive from left to right. Such a smooth distribution can be seen in the smallest tune of  $l = -1$  mode at  $\theta_p \geq 0.5$ . Although not shown here, the isolated  $l = 0$  mode exhibits a uniform dipole amplitude distribution.

Figure 3 presents the tune variation of beam-beam  $\pi$  modes as functions of bunch population.  $n_J$  points corresponding to  $J$  are seen for each azimuthal number in each  $N/N_0$ . The isolated mode seen in  $l = 0$  is the so-called  $\pi$  mode with flat radial distribution. Several isolated modes are seen in side bands. The isolated modes appear at the

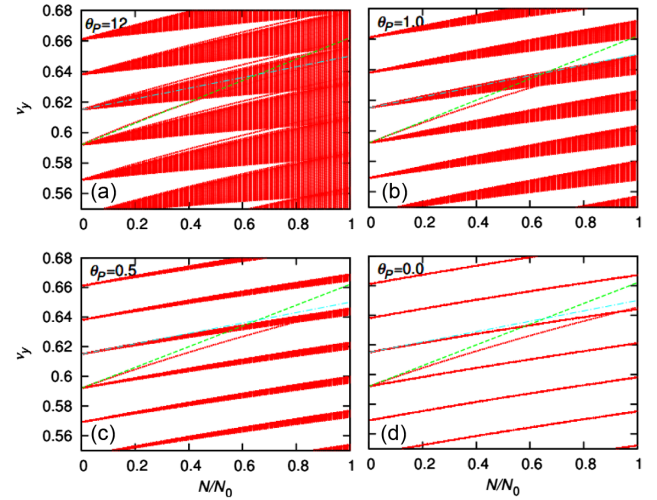


FIG. 3. Tune variation of beam-beam  $\pi$  modes for the beam-beam cross-wake force as functions of bunch population. Plots (a)–(d) show tune variation for  $\theta_p = 12, 1.0, 0.5, 0.0$ , respectively. Lines for  $\xi$  (green) and  $\xi/2$  (cyan) are drawn.

upper side of the tune spread for  $\theta_p = 12$ . The tune variation deviates from a straight line because it is obtained by solving for eigenvalues of the matrix.

## B. Combined effect of wake/impedance from a vacuum environment

The wake force induced by a vacuum boundary is added in the beam-beam cross-wake force. The magnitude of the wake force is characterized by the tune shift as a function of the bunch population. The tune shift is 0.015 at the positron bunch population  $N_0 = 9.3 \times 10^{10}$  which corresponds to  $\xi = 0.07$  for the collision. The threshold of the transverse mode coupling instability (TMCI) is  $N/N_0 = 1.4$ , where  $\nu_s = 0.023$ . Mode analysis is performed for various  $\theta_p$  with keeping the tune shift  $\Delta\nu/\xi = 0.015/0.07$ .

Figure 4 presents the tune variation of beam-beam  $\sigma$  modes for the total wake force of beam-beam and vacuum pipe environment. A similar tune variation as Fig. 1 is seen. Important is the variation of an isolated mode. The isolated mode at  $l = 0$  experiences a negative tune shift due to the wake force from the vacuum environment. The other isolated mode at  $l = -1$  does not change so much for the additional wake force at low bunch population  $N/N_0 \leq 0.5$ . This is a well-seen behavior in TMCI. Mode coupling appears at  $N/N_0 = 0.8$  for  $\theta_p = 12$ . For other  $\theta_p$ , mode coupling is seen, but modes separate at a higher population.

The mode analysis is again performed using simple radial mode in Eqs. (9) and (11). The eigenvalues are plotted in Fig. 4 as blue points. For  $l = 0$  and  $-1$  modes, the tunes completely agree with those of the isolated modes. There are some discrepancies in  $l \leq -2$  modes for the same reason as Fig. 1.

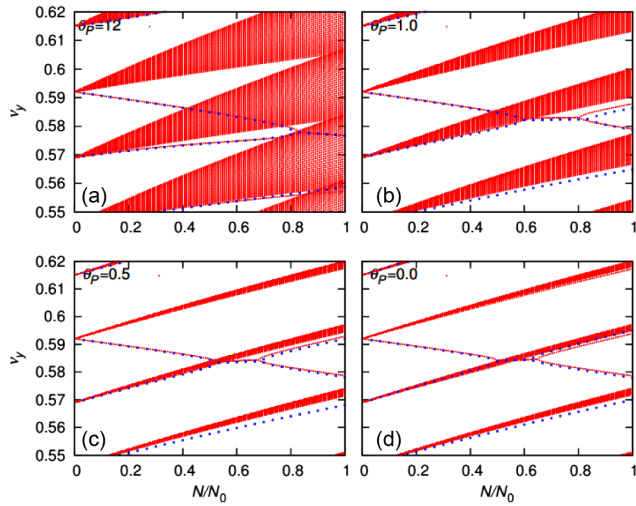


FIG. 4. Tune variation of beam-beam  $\sigma$  modes for the total wake force of beam-beam and vacuum pipe environment as functions of bunch population. Plots (a)–(d) show tune variation for  $\theta_p = 12, 1.0, 0.5, 0.0$ , respectively. The blue dots are given for the flat mode in Eqs. (9) and (11).

A similar analysis is performed for  $\pi$  modes as shown in Fig. 5. The tune range plotted is narrowed to visualize in more detail and the bunch population is increased to  $N/N_0 = 1.5$  to observe instability. A tune shift of the isolated  $\pi$  mode with  $l = 0$  which is somewhat small due to the impedance tune shift. No clear mode coupling is seen in the isolated modes, though the tunes cross each other for  $\theta_p = 12$  and 1. For  $\theta_p \leq 0.5$ , mode coupling between  $l = 0$  mode and  $+1$  mode is seen.

Figure 6 presents the growth rate for  $\theta_p = 12, 3.0, 1.0, 0.5, 0.0$ . Plot (a) depicts growth for  $\sigma$  mode. For smaller  $\theta_p$ ,

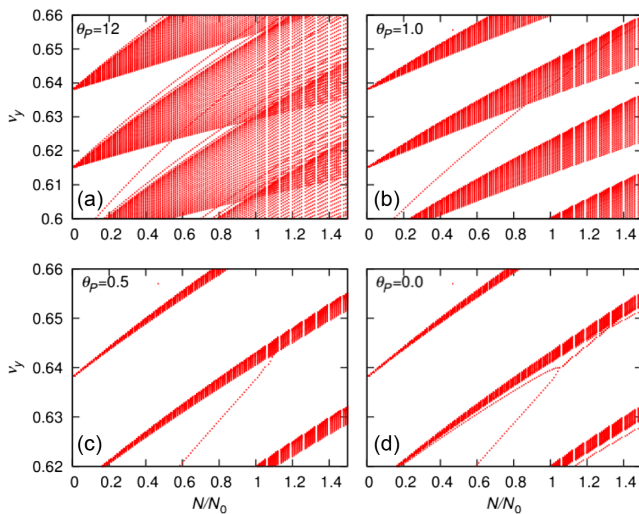


FIG. 5. Tune variation of beam-beam  $\pi$  modes for the total wake force of beam-beam and vacuum pipe environment as functions of bunch population. Plots (a)–(d) show tune variation for  $\theta_p = 12, 1.0, 0.5, 0.0$ , respectively.

mode coupling appears at lower population and stabilized at higher population. It makes sense that the threshold would be lower for smaller  $\theta_p$ , considering the flat mode tune shift varying from  $\xi/4$  to  $\xi/2$  in Eq. (13). The growth is faster for larger  $\theta_p$  under the condition of vacuum pipe impedance  $\Delta\nu/\xi = 0.015/0.07$ . The condition is not strict and depends on the accelerator design, so the growth rate should be seen as a reference. Unstable modes arise from the coupling between smooth modes as seen in Fig. 2(b) but not between continuous modes.

Plot (b) depicts growth for  $\pi$  mode. There are many cross points between modes as shown in Fig. 5. For  $\theta_p \leq 1$ , a clear growth, which corresponds to the mode coupling seen in Figs. 5(c) and 5(d), appears. For  $\theta_p = 12$ , a growth with a weak rate of  $\sim 0.001$  appears at  $N/N_0 = 0.55$ . This bunch population corresponds to that at which the flat 0 mode crosses the distributed  $+1$  mode (0.55, 0.63) in Fig. 5(a). The growth depends on the integration step  $n_J$ . This instability can be said to be an artifact of discretizing  $J$ , but it can also be said to be a result in a model that assumes coherence in the discretized region.

Figure 7 presents eigenvectors for the unstable  $\pi$  modes. Plot (a) is drawn for the weak growth mode in the coupling between the isolated 0 mode and continuously distributed  $+1$  mode as seen in Fig. 5(a), where  $\nu = 0.643$ ,  $N = N_0$ , and  $\theta_p = 12$ . The dipole distribution contains smooth dipole and thin skin components. Plot (b) is drawn for the clear growth mode in the coupling between isolated modes as seen in Fig. 5(c), where  $\nu = 0.646$ ,  $N/N_0 = 1.2$ ,

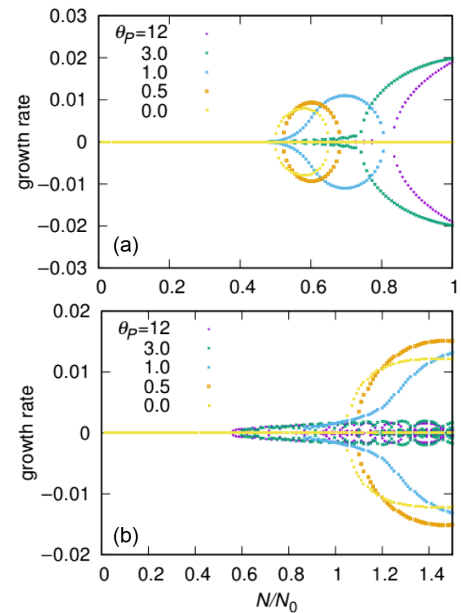


FIG. 6. Growth as functions of bunch population and  $\beta_y^*$ . Plots (a) shows the evolution of the vertical beam size for various bunch populations  $\xi$  and plot (b) shows the growth rate as a function of the bunch population for  $\beta_y \theta_p / \sigma_z = 1$  and 2, where  $\xi = 0.07$  for  $N/N_0 = 1$ .

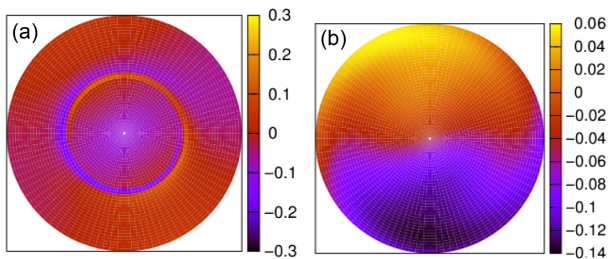


FIG. 7. Dipole amplitude distributions in the longitudinal phase space ( $\pm 2.45\sigma$ ) calculated by eigenvectors of unstable  $\pi$  modes. Plot (a) is drawn for the mode coupling at  $\nu = 0.643$ ,  $N = N_0$ , and  $\theta_p = 12$ . Plot (b) is drawn for the mode coupling at  $\nu = 0.646$ ,  $N/N_0 = 1.2$ , and  $\theta_p = 0.5$ .

and  $\theta_p = 0.5$ . The dipole distribution contains both smooth dipole and  $+1$  modes as seen in the offset of the scale. By the way, this smooth mode at the lower side of the tune spread does not exist only with the beam-beam interaction. The mode is formed by the wake force for only small  $\theta_p < 1$ .

It seems that whether the instability becomes obvious depends on whether the coupled modes are smooth or not. Such smooth modes are isolated from the continuous spectrum in this model. In order to form a smooth mode, the dipole moment must be correlated throughout the longitudinal phase space. On the other hand, the tune spread will inhibit that correlation. This can be a visualization of Landau damping.

### III. BEAM-BEAM SIMULATION CONSIDERING VACUUM ENVIRONMENT IMPEDANCE

Strong-strong beam-beam simulations have been performed to study the combined effects of beam-beam and vacuum pipe impedance. Vertical beam size blowup has been seen below the TMCI threshold [7]. The instability is understood as mode coupling between 0 and  $-1$  mode as discussed in the previous section. We here present strong-strong simulation results to sharpen the understanding of the beam-beam mode coupling.

The parameters used in the simulations are the same as those used in the analysis in Sec. II. The crossing angle  $\theta$  is 41.5–13.8 mrad also with changing the horizontal size ( $\sigma_x = 18$ –69  $\mu\text{m}$ ).  $\beta_x$  and  $\varepsilon_x$  are chosen so that the horizontal beam-beam instability [2] does not occur. The other parameters are chosen so that  $\xi$  and  $\sigma_z = 6$  mm are kept while changing  $\theta_p$ . The wake/impedance is added in both ( $e^\pm$ ) rings with an equal tune shift for  $\xi$ . The IP vertical beta function normalized by the overlap area is  $\theta_\beta \equiv \beta_y^* \theta_p / \sigma_z = 2.3$  ( $\beta_y^* = 1$  mm) at the reference condition.

Figure 8 presents the oscillation of two beams,  $\langle y \rangle / \sigma_y$  and  $\langle yz \rangle / \sigma_y \sigma_z$ , at the appearance of the instability. Both beams oscillate at the same betatron phase in both  $f \langle y \rangle$  and  $\langle yz \rangle$  with considerable amplitudes  $\sim 0.1\sigma_y$ . This means that  $\sigma$  mode of beam-beam instability occurs. The threshold of

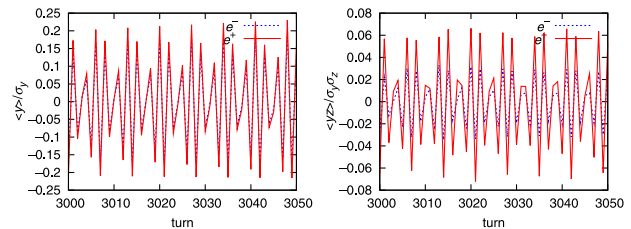


FIG. 8. Vertical oscillation amplitude of both beams,  $\langle y \rangle / \sigma_y$  and  $\langle yz \rangle / \sigma_y \sigma_z$  in the instability occurrence.

the instability was  $N/N_0 = 0.7$  for  $\theta_p = 12$ , which is in close agreement with the mode analysis. The growth rate was 0.007 for  $N = N_0$ , which was 1/3 of the mode analysis result 0.02. The nonlinear beam-beam force probably slows down the growth.

The instability should be independent of the vertical tune under the condition that the tunes of the two beams are equal. Figure 9(a) shows the growth rate of dipole amplitude scanning  $\nu_y = 0.555$ –0.595 and does not change for  $\nu_y > 0.56$  as expected. The growth is lower at  $\nu_y = 0.555$  and 0.56. There may be some reason to suppress the instability at the low tune. Figure 9(b) shows the growth rate of dipole amplitude as a function of the normalized beta for the overlap area,  $\beta_y \theta_p / \sigma_z$ , where  $\theta_p = 12$ . The normalized beta characterizes the hourglass effect in collision with  $\theta_p \geq 1$ . For  $\beta_y \theta_p / \sigma_z = 0.77$ , the growth rate decreases 10%. The hourglass effect on this instability is weak for  $\beta_y \theta_p / \sigma_z \geq 1$ .

We next discuss the growth as a function of the bunch population for  $\theta_p = 1$  seen in Fig. 6(a). Figure 10 presents the growth of the instability for  $\beta_y \theta_p / \sigma_z = 2$  and 1. Plot (a) shows the evolution of  $\sigma_y$  for various  $N/N_0$ . The instability is seen at a range of  $N/N_0 = 0.5$ –0.7 for  $\beta_y \theta_p / \sigma_z = 2$ , while is seen at  $N/N_0 = 1$  for  $\beta_y \theta_p / \sigma_z = 1$ . An incoherent emittance growth is also seen for  $\beta_y \theta_p / \sigma_z = 1$ . Plot (b) shows the growth rate as a function of  $N/N_0$ , where  $\xi = 0.07$  at  $N/N_0 = 1$ . For  $\beta_y \theta_p / \sigma_z = 1$ , the growth of the instability increases monotonically. The incoherent emittance growth occurs due to the hourglass effect. It seems that the instability appears at  $N/N_0 = 1$  since the emittance growth reduces the beam-beam parameter effectively.

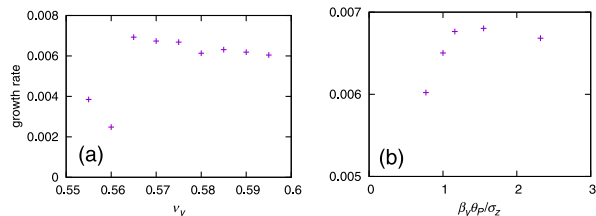


FIG. 9. Growth rate as functions of (a) vertical tune and (b)  $\beta_y \theta_p / \sigma_z$  for  $\theta_p = 12$ .

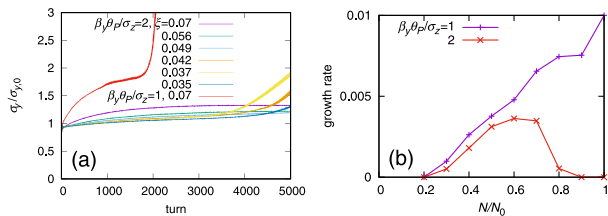


FIG. 10. Growth for  $\theta_p = 1$ . (a) Evolution of  $\sigma_y$  for various growth rate as a function of (a)  $\beta_y$  and (b).

#### IV. CONCLUSIONS

We have discussed the beam-beam mode and instability for collision with a crossing angle in the presence of vacuum environment wake/impedance. The beam-beam mode is defined by expanding the dipole amplitudes in the longitudinal phase space to azimuthal and radial directions. The modes of colliding beams were first obtained by considering only the beam-beam interaction. Applying the transparency condition,  $\sigma$  and  $\pi$  modes can be treated with independent equations. The tune of each mode was calculated as eigenvalues for the dipole amplitude of two beams correlated by the cross-wake force. There were continuously distributed radial modes with tune  $\nu_l(J)$  for the longitudinal amplitude  $J$  in each azimuthal mode  $l$ . The tune spread for  $J$  is wider for larger  $\theta_p$ . All radial modes are degenerated at  $\theta_p = 0$ . Clear isolated  $\sigma$  modes for  $l = 0$  and  $-1$  are seen at  $\theta_p > 1$ . Isolated modes are also found in  $\pi$  mode. In such isolated modes, the dipole amplitude is smoothly distributed in the longitudinal phase space.

The beam-beam interaction does not cause instability in low azimuthal (synchrotron side band) modes, though tunes of the modes cross each other with increasing bunch population. This is due to the cross-wake force is symmetric for  $z$  and the impedance is pure imaginary.

The wake/impedance from the vacuum environment deforms the mode. The total wake is not now symmetric for  $z$  which means the impedance contains real part. The isolated dipole mode  $l = 0$  also experiences a negative tune shift due to the wake/impedance.

The breaking of the symmetry and the negative tune shift have a strong impact on TMCI in  $\sigma$  mode. The isolated modes  $l = 0$  and  $l = -1$  merge at a lower bunch population then mode coupling instability occurs. We conclude that the beam-beam interactions lower the threshold of TMCI.

The threshold of the mode coupling between the isolated modes (0 and  $-1$ ) is lower when  $\theta_p$  is smaller. This is because the tune shift of the isolated  $l = -1$  mode is  $\xi/2$  when  $\theta_p$  is small, and  $\xi/4$  when  $\theta_p$  is large. The growth rate depends on the accelerator design.

For  $\pi$  mode, mode coupling between isolated modes occurs at a higher bunch population than in  $\sigma$  mode. A isolated 0 mode couples to an isolated  $+1$  mode which is induced by the vacuum environment wake force.

There are continuously distributed modes  $\nu(J)$  as function of  $J$ . Mode coupling between distributed modes is weak or nonexistent.

Strong-strong simulations including vacuum environment impedance showed some results validating the mode analysis: (i)  $\sigma$  mode was seen in  $\langle y \rangle$  and  $\langle yz \rangle$ , when the instability occurred; (ii) the instability threshold was  $N/N_0 = 0.7$  for  $\theta_p = 12$ , which is in close agreement with the mode analysis ( $N/N_0 = 0.8$ ); (iii) the growth rate of 0.007 was 1/3 of the mode analysis 0.02, but considering the nonlinearity of the beam-beam force, it was reasonable; (iv) the growth of the instability was independent of  $\nu_y$ , except for lower tune  $\nu_y \sim 0.55$ ; (v) hourglass effect, which was not considered in the mode analysis, basically had little effect on the instability for  $\beta_y \theta_p / \sigma_z \geq 1$ ; and (vi) emittance growth caused by the hourglass effect could result in the instability due to the corresponding reduction of  $\xi$  only for small  $\theta_p \leq 1$ .

Considering high azimuthal modes, tunes are wrapped at the half-integer and coupled to nonwrapped modes. Instability can occurs even only beam-beam interaction as shown in the horizontal [7]. Strong-strong simulations do not show the instability. Perhaps the instability is smeared by the strong nonlinear force of the beam-beam interaction.

#### ACKNOWLEDGMENTS

The work is funded by the Chinese Academy of Sciences President's International Fellowship Initiative (Grant No. 2019VMA0034) and Innovation Study of IHEP. We thank to Professor E. Forest for reading of this manuscript.

- [1] A. Chao, *Physics of Collective Beam Instabilities in High Energy Accelerators*, (Wiley-Interscience Publication, New York, 1993), and references therein.
- [2] K. Ohmi, N. Kuroo, K. Oide, D. Zhou, and F. Zimmermann, *Phys. Rev. Lett.* **119**, 134801 (2017).
- [3] N. Kuroo, K. Ohmi, K. Oide, D. Zhou, and F. Zimmermann, *Phys. Rev. Accel. Beams* **21**, 031002 (2018).
- [4] C. Lin, K. Ohmi, and Y. Zhang, *Phys. Rev. Accel. Beams* **25**, 011001 (2022).
- [5] Y. Zhang, in *Proceedings of the 1st CEPC International Accelerator Review Committee Meeting in 2022, Beijing, China, 2022* (2022), <https://indico.ihep.ac.cn/event/16801/>.
- [6] K. Ohmi and Y. Zhang, SuperKEKB International Task force beam-beam subgroup meetings, <https://kds.kek.jp/event/40786/> and <https://kds.kek.jp/event/42908/>.
- [7] Y. Zhang, N. Wang, K. Ohmi, D. Zhou, T. Ishibashi, and C. Lin, *Phys. Rev. Accel. Beams* **26**, 064401 (2023).
- [8] D. Zhou, K. Ohmi, Y. Funakoshi, Y. Ohnishi, and Y. Zhang, *Phys. Rev. Accel. Beams* **26**, 071001 (2023).
- [9] E. A. Perevedentsev and A. A. Valishev, *Phys. Rev. ST Accel. Beams* **4**, 024403 (2001).
- [10] S. White, X. Buffat, N. Mounet, and T. Pieloni, *Phys. Rev. ST Accel. Beams* **17**, 041002 (2014).
- [11] A. Piwinski, DESY Report No. DESY 77/18, 1977, <https://lib-extopc.kek.jp/preprints/PDF/1977/7706/7706148.pdf>.